12-Lipoxygenase inhibition suppresses islet immune and inflammatory responses and delays autoimmune diabetes in human gene replacement mice

Titli Nargis[1], Charanya Muralidharan[1], Jacob R. Enriquez[1], Jiayi E. Wang[1], Kerim Kaylan[1], Advaita Chakraborty[1], Sarida Pratuangtham[1], Kayla Figatner[1], Jennifer B. Nelson[1], Sarah C. May[1], Jerry L. Nadler[2], Matthew B. Boxer[3], David J. Maloney[3], Sarah A. Tersey[1,*], and Raghavendra G. Mirmira[1,*]

[1]Department of Medicine and the Kovler Diabetes Center, The University of Chicago, Chicago, IL 60637, USA

[2]Department of Pharmacology, New York Medical College, Valhalla, NY 10595, USA

[3]Veralox Therapeutics, Frederick, MD 21704, USA

***Corresponding authors**: Sarah A. Tersey (stersey@uchicago.edu) 900 E. 57th Street, KCBD 8152, Chicago, IL 60637 USA and Raghavendra G Mirmira (mirmira@uchicago.edu), 900 E. 57th Street, KCBD 8130, Chicago, IL, 60637 USA.

Key Words: type 1 diabetes, islet, macrophage, autoimmunity, lipoxygenase, mouse model

Disclosures: RGM and SAT received an investigator-initiated award from Veralox Therapeutics. RGM serves on the Scientific Advisory Board for Veralox Therapeutics. DJM and MBB are Veralox Therapeutics employees.

ABSTRACT

Type 1 diabetes (T1D) is characterized by the autoimmune destruction of insulin-producing β cells and involves an interplay between β cells and cells of the innate and adaptive immune systems. We investigated the therapeutic potential of targeting 12-lipoxygenase (12-LOX), an enzyme implicated in inflammatory pathways in β cells and macrophages, using a mouse model in which the endogenous mouse *Alox15* gene is replaced by the human *ALOX12* gene. Our findings demonstrate that VLX-1005, a potent 12-LOX inhibitor, effectively delays the onset of autoimmune diabetes in human gene replacement non-obese diabetic mice. By spatial proteomics analysis, VLX-1005 treatment resulted in marked reductions in infiltrating T and B cells and macrophages with accompanying increases in immune checkpoint molecule PD-L1, suggesting a shift towards an immune-suppressive microenvironment. RNA sequencing analysis of isolated islets and polarized proinflammatory macrophages revealed significant alteration of cytokine-responsive pathways and a reduction in interferon response after VLX-1005 treatment. Our studies demonstrate that the *ALOX12* human replacement gene mouse provides a platform for the preclinical evaluation of LOX inhibitors and supports VLX-1005 as an inhibitor of human 12-LOX that engages the enzymatic target and alters the inflammatory phenotypes of islets and macrophages to promote the delay of autoimmune diabetes.

45 **INTRODUCTION**

46 The pathogenesis of type 1 diabetes (T1D) involves a complex interplay between
47 multiple cell types within the pancreatic islet, including innate immune cells (macrophages,
48 dendritic cells), insulin-producing cells (β cells), and adaptive immune cells (T cells, B cells)
49 (1). Although the disease has traditionally been viewed as arising from a primary defect in
50 immune tolerance, an emerging perspective posits that environmental factors (such as
51 viruses or other systemic inflammatory disorders) may aggravate an interaction between
52 macrophages and β cells, facilitating oxidative and endoplasmic reticulum (ER) stress
53 pathways in β cells (2–4). These pathways facilitate the generation of β-cell neoepitopes
54 that then trigger adaptive autoimmunity (5, 6). Disease-modifying therapies—those that alter
55 disease pathogenesis rather than correcting the underlying disease phenotypes—have
56 largely focused on the adaptive immune system and seen some successes in clinical trials.
57 For example, an anti-CD3 monoclonal antibody (teplizumab) that targets activated T cells
58 has been shown to delay the onset of T1D by up to two years in subjects at high risk for the
59 disease (7). Given the increasing appreciation of innate immune cells and β cells in early
60 T1D pathogenesis, the identification of drugs targeting these cell types raises the possibility
61 that combination therapeutic approaches may provide more durable outcomes.

62 The lipoxygenases (LOXs) encompass a family of enzymes involved in lipid
63 metabolism that facilitates the oxygenation of polyunsaturated fatty acids to form
64 eicosanoids, some of which are pro-inflammatory in nature (8). In the mouse, 12/15-LOX is
65 encoded by the *Alox15* gene and is the primary active LOX present in macrophages and β
66 cells and produces the proinflammatory eicosanoid 12-hydroxyeicosatetraenoic acid (12-
67 HETE) as a principal product from the substrate arachidonic acid (9). Whole-body deletion of
68 *Alox15* on the autoimmune non-obese diabetic (NOD) mouse background results in almost
69 complete protection against diabetes (10). Deletion of *Alox15* in either the innate immune
70 myeloid cells (2) or in β cells (11) recapitulates the autoimmune diabetes protection seen in
71 the whole-body deletion, emphasizing both the early role of these cell types in T1D and the
72 importance of the 12/15-LOX pathway in disease pathogenesis. In these cell-specific

73 deletion models, islets exhibit marked reductions in invading pathogenic T cells (insulitis), a
74 finding reflecting the disease-modifying response. The molecular events tied to disease
75 protection ostensibly emanate from reductions in oxidative and ER stress (and the resultant
76 reduction in neoepitope formation and presentation) as well as from enhanced display of PD-
77 L1 (an immune-suppressive checkpoint ligand) on the surface of myeloid cells and β cells (2,
78 11).
79 In humans, the relevant LOX enzyme that produces 12-HETE is 12-LOX, encoded by
80 the *ALOX12* gene. Like the mouse 12/15-LOX, human 12-LOX is present in residual insulin-
81 positive cells in donors with T1D or in autoantibody-positive donors at risk for T1D (12)—a
82 finding consistent with a potential role in promoting β-cell sensitivity to autoimmunity. A
83 major challenge to using mice as a platform to test inhibitors is that human 12-LOX exhibits
84 structurally distinct characteristics from mouse 12/15-LOX, thereby necessitating the
85 development of different inhibitors that cannot be tested for efficacy in mice (13–15).
86 Previously, VLX-1005 (also known as ML355) was described as a potent and selective
87 inhibitor of human 12-LOX while also displaying a favorable half-maximal inhibitory
88 concentration (IC_{50}) and pharmacokinetic (PK) properties (16). VLX-1005 was shown to
89 protect human islets in vitro against dysfunction caused by proinflammatory cytokines (17),
90 but the lack of appropriate in vivo model systems has made it challenging to
91 pharmacologically validate VLX-1005 as a therapeutic target in autoimmune diabetes. To
92 address this challenge, we developed new mouse strains in which the mouse *Alox15* gene is
93 replaced by the human *ALOX12* gene while retaining the mouse gene's upstream control
94 elements. This human gene replacement platform was leveraged to test if and how human
95 12-LOX pharmacologic inhibition of human 12-LOX with VLX-1005 modifies disease
96 progression in autoimmune T1D.
97
98 **RESULTS**
99 ***Generation and validation of the hALOX12 gene replacement mouse model***

100 To establish a platform to test potential inhibitors of human 12-LOX in vivo, we
101 generated a mouse model in which the endogenous mouse *Alox15* gene is replaced by the
102 human *ALOX12* gene (**Figure 1A**). This model leaves the mouse upstream regulatory region
103 intact to ensure that the expression of *ALOX12* recapitulates the expression of *Alox15*.
104 These mice (henceforth referred to as *hALOX12* mice) were introgressed onto the *C57BL/6J*
105 mouse background using a speed congenics approach and bred to homozygosity.
106 Microsatellite genotyping showed that the mice were 100% congenic on the *C57BL/6J* (or
107 simply *B6*) background (**Supplemental Table 1** Excel file). To confirm the successful
108 deletion of mouse *Alox15* and replacement with human *ALOX12*, we performed standard
109 genotyping (**Supplemental Figure 1A**). Additionally, we isolated tissues (kidney, spleen,
110 lung, fat, liver, islets, peritoneal macrophages, and bone marrow-derived macrophages
111 (BMDMs)) from wildtype *B6* and *B6.hALOX12* mice and subjected them to gene expression
112 analysis for *Alox15* and *ALOX12.* As anticipated, wildtype tissues expressed mouse *Alox15*
113 and did not express human *ALOX12*; conversely, *B6.hALOX12* mice tissues expressed
114 *ALOX12* but not *Alox15* (**Table 1**).
115 Because lipoxygenases are known to affect metabolic function, we next performed
116 metabolic characterization to determine if/how the replacement of *Alox15* with *ALOX12*
117 altered metabolic phenotypes. We found no significant differences in body weight, lean
118 mass, fat mass, random-fed blood glucose levels, or glucose tolerance between wildtype *B6*
119 and *B6.hALOX12* mice (**Supplemental Figure 1B-F**). Moreover, islet ultrastructure (relative
120 immunostaining patterns of α cells and β cells) and composition (α cell mass and β cell
121 mass) were indistinguishable between 10 week-old wildtype and *B6.hALOX12* mice
122 (**Supplemental Figure 1G-I**). Taken together, these data suggest that the successful
123 replacement of *Alox15* with human *ALOX12* did not alter gross metabolic or islet
124 phenotypes.
125
126 ***Effects of VLX-1005 against STZ-induced diabetes are specific to B6.hALOX12 mice***

127 Prior studies demonstrated that whole-body deletion of mouse *Alox15* protects
128 against diabetes induced by the chemical streptozotocin (STZ) (18). To test if the human 12-
129 LOX inhibitor VLX-1005 (14) (**Figure 1B**) phenocopies deletion of the enzyme in our human
130 gene replacement mice, we employed a similar STZ diabetes induction protocol. STZ is a β
131 cell toxin that induces low-grade inflammation, macrophage influx into islets, and eventual
132 diabetes in mice after 5 daily low-dose intraperitoneal injections (55 mg/kg) (19). Eight-week-
133 old male wildtype *B6* and *B6.hALOX12* mice were injected intraperitoneally daily with vehicle
134 or 30 mg/kg VLX-1005 in the peri-STZ treatment period (for the 5 days before, during, and
135 after STZ). STZ-injected *B6* and *B6.hALOX12* mice receiving vehicle became overtly
136 hyperglycemic within 10 days of starting STZ treatment and displayed equivalent glucose
137 intolerance by GTT (**Figure 1C and D**). Upon receiving VLX-1005, however, *B6.hALOX12*
138 mice showed complete protection from STZ-induced diabetes, whereas wildtype *B6* mice
139 became overtly hyperglycemic (**Figure 1E**); GTTs at the end of the study confirmed
140 improved glucose tolerance in *B6.hALOX12* mice compared to wildtype *B6* mice (**Figure 1F**
141 **and G**). These data indicate a specific effect of the drug in preventing hyperglycemia in
142 *B6.hALOX12* mice and support the effectiveness of the *hALOX12* platform for interrogating
143 VLX-1005 action.
144
145 ***Pharmacokinetics of oral VLX-1005 and its effects on STZ-induced diabetes***
146 Given that the oral route is the preferred route for systemic drug delivery in humans,
147 we next asked if oral administration of VLX-1005 provides adequate exposure in mice. We
148 performed pharmacokinetic analysis following a single oral administration (as a suspension
149 in 0.5% methylcellulose) of VLX-1005 spray dried dispersion at a dose of 30 mg/kg in
150 C57BL/6J mice, followed by serial analysis of VLX-1005 levels by LC-MS/MS. The
151 pharmacokinetic profile of orally-administered VLX-1005 in mice shows a mean half-life ($T_{1/2}$)
152 of 3.24 ± 0.07 hours and a consistent T_{max} of 0.250 hours across all mice. The C_{max} was
153 13300 ± 624 ng/ml, with moderate variability in AUC (15029 ± 3177 h*ng/ml). These
154 parameters, particularly the low variability in T_{max} and C_{max}, support the feasibility of once-

155 daily dosing for maintaining therapeutic levels over a 24-hour period (**Table 2**). We next
156 tested the effects of oral administration of VLX-1005 on the low-dose STZ model, with VLX-
157 1005 (at 30 mg/kg) given 3 days prior to the start of STZ, during STZ, and for 3 days
158 following STZ treatment. Similar to intraperitoneal delivery, oral administration of VLX-1005
159 in *B6.hALOX12* mice resulted in lower random-fed blood glucose levels (**Figure 1H**) and
160 significantly improved glucose tolerance (**Figure 1I and J**) compared to vehicle—although
161 this effect was not as robust as with intraperitoneal delivery of the drug. Consistent with
162 improved glucose homeostasis, oral VLX-1005-treated mice exhibited greater β cell mass at
163 the end of the study compared to vehicle-treated mice (**Figure 1K**). Collectively, these data
164 suggest that a single daily oral delivery of VLX-1005 (at 30 mg/kg) achieves plasma levels
165 with therapeutic efficacy.
166
167 ***VLX-1005 treatment reduces β cell inflammation in NOD.hALOX12 mice***
168 The non-obese diabetic (*NOD*) mouse model is a model of T1D that recapitulates
169 many of the immune and β cell features of the disease (20). We, therefore, asked if
170 pharmacologic inhibition of 12-LOX using orally administered VLX-1005 protects against
171 spontaneous diabetes development in the *NOD* mouse model. To address this question, we
172 introgressed humanized *hALOX12* mice onto the *NOD* background using a speed congenics
173 approach. Genome scanning of microsatellites was performed to confirm that mice were
174 100% congenic on the *NOD* mouse background (*NOD.hALOX12* mice) (**Supplemental**
175 **Table 1** Excel file). We next measured human 12-LOX protein levels in the *NOD.hALOX12*
176 mice. Similar to the gene profile we observed in *B6.ALOX12 mice* compared to wildtype
177 *C57BL/6J* mice, wildtype *NOD* tissues robustly expressed mouse 12/15-LOX (the protein
178 encoded by mouse *Alox15*) and little/no human *ALOX12*; conversely, *NOD.hALOX12* mice
179 tissues robustly expressed human 12-LOX and minimal levels of 12/15-LOX (**Supplemental**
180 **Figure 1J and 1K**). Consistent with their congenic nature, female *NOD.hALOX12* mice
181 exhibited islet pathology similar to *NOD* mice at the (prediabetic) age of 10 weeks with
182 evidence of T and B cell infiltration of islets (**Supplemental Figure 1L**) and indistinguishable

183 insulitis score (**Supplemental Figure 1M)**, suggesting that replacement of *Alox15* with
184 human *ALOX12* did not alter the islet pathology of the disease. Pharmacokinetics of orally
185 administered VLX-1005 (30 mg/kg) on the *NOD* background were similar to those seen in
186 *C57BL/6J* mice (**Table 2**), suggesting that the *NOD* background does not affect drug
187 absorption or clearance.

188 To assess the effect of VLX-1005 administration on products of 12-LOX activity in
189 *NOD.hALOX12* mice, we administered 30 mg/kg VLX-1005 (or vehicle) orally to female
190 *NOD.hALOX12* mice for 1 week during the pre-diabetic phase (8 weeks of age) and
191 harvested serum. Lipidomics analysis (by LC/MS/MS) was performed for a series of 12-LOX
192 products resulting from different fatty acid substrates (**Figure 2A**). Notably, levels of 12-
193 HETE (from arachidonic acid), 13-HODE (from linoleic acid), and 14-HDHA and 17-HDHA
194 (from docosahexaenoic acid) were all significantly reduced (**Figure 2B**). Levels of 12-HEPE
195 (from eicosapentaenoic acid) were not significantly changed (**Figure 2B**), suggesting
196 minimal involvement of eicosapentaenoic acid metabolism in *NOD* mice. Lipids within the
197 pathway that are processed by enzymes other than 12-LOX were not statistically
198 significantly altered (**Supplemental Table 2**). These data are collectively consistent with the
199 expected 12-LOX engagement by VLX-1005.

200 To assess the effect of VLX-1005 administration on immune cell phenotypes in
201 *NOD.hALOX12* mice, we administered 30 mg/kg VLX-1005 (or vehicle) orally to female
202 *NOD.hALOX12* mice for 4 weeks during the pre-diabetic phase (6-10 weeks of age) and
203 harvested pancreas, pancreatic lymph nodes (pLNs), and spleen (**Figure 2C**). Pancreas
204 pathology showed reduced T and B cell infiltration and that the extent of insulitis (by insulitis
205 scoring) was significantly reduced in VLX-1005-treated *NOD.hALOX12* mice compared to
206 vehicle-treated mice (**Figure 2D-E**). To specifically interrogate the nature of immune cells
207 within the insulitic region, we performed spatial tissue-based proteomics (Nanostring®). We
208 used insulin immunostaining and nuclei staining to identify β cells and the surrounding
209 insulitic regions. Pre-validated antibodies in the GeoMx® mouse immune panel were used to
210 probe for immune cell subtypes in the peri-islet insulitic region and within the islet.

211 *NOD.hALOX12* mice exhibited a notable reduction of myeloid population subtypes in both
212 insulitic and islet areas, including macrophages (F4/80+; CD11b+) and dendritic cells
213 (CD11c+) (**Figure 2F** and **Supplemental Figure 2A-B**). This reduction in myeloid cell
214 populations was accompanied by a decrease in T and B cells populations, including CD4+,
215 CD3+, CD8+, and CD19+ cells (**Figure 2F** and **Supplemental Figure 2A-B**).
216 Immunohistochemistry of pancreas sections confirmed the reductions in both T cells (CD3+),
217 macrophages (F4/80+), and activated macrophages (Mac2+) following oral VLX-1005
218 treatment (**Figure 2G**). A notable observation in spatial proteomics was the increased levels
219 of the immune checkpoint ligand PD-L1 (**Figure 2F**). Enhanced PD-L1/PD-1 interactions
220 shift T cells to less aggressive, more regulatory phenotypes (21). To interrogate this
221 possibility, we performed immune profiling by flow cytometry of pancreatic lymph nodes
222 (pLNs) from mice treated with oral VLX-1005 or vehicle. pLNs are key sites in the initial
223 priming of autoreactive T cells in *NOD* mice (22). Treatment with oral VLX-1005 led to an
224 increase in CD4+Foxp3+ regulatory T cells (Tregs) in the pLNs (**Supplemental Figure 2C**).
225 This effect on Tregs was specific for the pLNs since no changes in Tregs were observed in
226 the spleen after VLX-1005 treatment (**Supplemental Figure 2D**).
227
228 ***Orally-administered VLX-1005 reduces autoimmune diabetes incidence in female and***
229 ***male NOD.hALOX12 mice***
230 Because 4 weeks of oral VLX-1005 dosing led to improvements in insulitis and
231 reductions in infiltrating T and B cells, we next asked if these alterations lead to prevention or
232 delay of subsequent diabetes development in *NOD.hALOX12* mice. Both female and male
233 mice were administered VLX-1005 via daily oral gavage (30 mg/kg) or vehicle for 4 weeks
234 during the pre-diabetic phase (6-10 weeks of age). Mice were followed for diabetes
235 development (blood glucose ≥250 mg/dl on 2 consecutive days) until 25 weeks of age
236 (**Figure 3A**). At 25 weeks of age, 60% of female mice and 75% of male mice receiving VLX-
237 1005 were protected from diabetes development compared to 25% of female and 50% of
238 male mice receiving vehicle (**Figure 3B-C**). Whereas the preceding studies demonstrate that

239 12-LOX inhibition with oral VLX-1005 delays the development of diabetes, they do not
240 address if administration of the drug might reverse established diabetes or mitigate
241 hyperglycemia. We allowed female *NOD.hALOX12* mice to develop diabetes (defined as 2
242 consecutive random-fed blood glucose measurements ≥250 mg/dL), then administered VLX-
243 1005 or vehicle for up to 6 weeks via daily oral gavage or until the mice exhibited signs of
244 physical deterioration from hyperglycemia (loss in body weight, dishevelment) (**Figure 3D**).
245 Notably, we did not observe a reversal in diabetes but did see relative reductions in blood
246 glucose levels in mice treated with VLX-1005 compared to vehicle (**Figure 3E-F**).
247
248 ***Orally-administered VLX-1005 reduces islet death and oxidative stress in***
249 ***NOD.hALOX12 mice***
250 12-LOX is primarily present in islets and macrophages, and deletion of the mouse
251 gene (*Alox15*) in either tissue separately was previously shown to reduce diabetes
252 incidence. We, therefore, first asked how treatment with VLX-1005 affects islet cell
253 phenotypes. We first subjected isolated islets from female *NOD.hALOX12* mice treated with
254 vehicle or VLX-1005 to RNA sequencing to identify how islet gene expression might be
255 altered. Principal component analysis of transcriptomics revealed that islets from vehicle-
256 and VLX-1005-treated *NOD.hALOX12* mice clustered separately, suggesting an effect of
257 VLX-1005 treatment on gene expression (**Figure 4A**). Pairwise comparison of gene
258 expression using a false discovery rate (FDR)<0.05 and fold-change (FC)>2 yielded only
259 189 differentially expressed genes. Instead, a P<0.05 cutoff and FC>2 revealed alteration of
260 709 genes between vehicle- and VLX-1005-treated *NOD.hALOX12* mice (**Figure 4B**,
261 volcano plot and **Supplemental Table 3** Excel file for full sequencing results). Gene
262 Ontology pathway analysis showed significantly altered pathways related to DNA replication
263 (e.g. *Anp32b, Skp1a, Itfg2, Dmrt1i*), inflammation (NFκB activity) (e.g. *Elf1, Trim75, RNase1,*
264 *Lmo1, Bcl3, Ptgis, Commd1, Lrrc14, Foxp3*), and G-protein coupled receptor signaling (e.g.
265 *Gpr89, Glp2r*), among others (**Figure 4C**). These pathways suggest responses that may be
266 related to changes in cellular survival in response to VLX-1005. We, therefore,

267 immunostained pancreatic sections for markers of cell death and proliferation in the islet.
268 VLX-1005-treated *NOD.hALOX12* mice exhibited decreased islet cell death as measured by
269 reduced terminal deoxynucleotidyl transferase dUTP nick end labeling (TUNEL) and H2A
270 histone family member X (H2A.X) staining compared to vehicle-treated mice (**Figure 4D**).
271 Additionally, VLX-1005-treated mice demonstrated decreased β cell proliferation, as
272 measured by proliferating cell nuclear antigen (PCNA) immunostaining (**Figure 4D**); reduced
273 PCNA immunostaining was also consistent with the reduction of Ki67 observed in spatial
274 proteomics of the insulin+ area (**Figure 2F** and **Supplemental Figure 2B**). We interpret the
275 reduction in β cell proliferation as a consequence of reduced β cell apoptosis. The alteration
276 in NFκB signaling led us to investigate if markers of oxidative stress were affected since
277 inflammation, oxidative stress, and β cell survival are closely linked (23, 24). We performed
278 immunostaining for the oxidative stress marker, 4-hydroxynonenal (4-HNE) and observed
279 reduced immunostaining in mice treated with VLX-1005 compared to placebo (**Figure 4E**).
280 Consistent with this observation, β cells from VLX-1005-treated animals also displayed an
281 increase in levels of the antioxidant enzyme GPx1 (**Figure 4E**). Collectively, these data are
282 consistent with prior observed effects of reduced inflammation, oxidative stress, and β cell
283 death in β cell-specific deletion of mouse *Alox15* in NOD mice (11).
284
285 ***VLX-1005 alters the proinflammatory macrophage phenotype***
286 Whereas the preceding findings are consistent with improved β cell survival following
287 oral VLX-1005 administration, these studies do not rule out the possibility that the drug
288 directly modifies the phenotype of infiltrating macrophages, which could secondarily affect β
289 cells. Because bulk islet transcriptomics analysis does not resolve gene expression events
290 associated with specific cell types, we isolated bone marrow-derived macrophages (BMDMs)
291 from female *NOD.hALOX12* mice and then performed RNA sequencing in the presence or
292 absence of VLX-1005. BMDMs were unpolarized ("M0") or polarized to an "M1-like" state
293 (with lipopolysaccharide and IFN-γ) to mimic the inflammatory state that might be observed
294 during T1D pathogenesis. During polarization, BMDMs were treated with vehicle or VLX-

295 1005 (**Figure 5A**). Principal component analysis of transcriptomics revealed that M0
296 macrophages treated with VLX-1005 co-clustered with vehicle-treated M0 macrophages,
297 suggesting a minimal transcriptional effect of the drug on unpolarized cells (**Figure 5B**).
298 Consistent with this interpretation, only 1% of genes (159 out of 15,888) were significantly
299 altered with VLX-1005 treatment (when using criteria FC>2 and P<0.05) (**Supplemental**
300 **Table 4** Excel file for full sequencing results). Upon polarization to the M1-like state, a clear
301 rightward shift in the principal component analysis plot was observed with both vehicle and
302 VLX-1005-treated BMDMs and a notable separation was seen between vehicle and VLX-
303 1005 treatment (**Figure 5B**); this finding suggests that the impact of 12-LOX inhibition is
304 more prominent upon a shift to a proinflammatory state of macrophages.
305 We next interrogated the gene expression events associated with the M0 to M1
306 transition in both vehicle and VLX-1005-treated BMDMs. Most genes altered (FC>2 and
307 P<0.05) in this transition (2467) were common between vehicle and VLX-1005 treatment
308 (**Figure 5C-D**, **Supplemental Figure 3A,** and **Supplemental Table 4** Excel file). These
309 common genes mapped to pathways related to cytokine-mediated signaling, T cell
310 activation, and antigen processing and presentation (**Supplemental Figure 3B**). An
311 additional 507 genes were significantly altered in vehicle-treated cells, and 459 additional
312 genes were significantly altered with VLX-1005 treatment (**Supplemental Figure 3A**). The
313 507 genes altered with vehicle treatment mapped to GO pathways related to the M1
314 polarization phenotype (myeloid cell differentiation, immune response, response to
315 cytokines) and pathways related to oxidative stress (cell redox homeostasis, response to
316 hydrogen peroxides) (**Figure 5E**). These pathways were not identified in the genes that were
317 differentially expressed during VLX-1005 treatment. GO pathway analysis of the 459 genes
318 altered with VLX-1005 showed particularly significant alterations in pathways related to
319 modification of the interferon response (**Figure 5F**). Next, we looked specifically at the genes
320 that mapped to interferon pathways (**Figure 5G**), which revealed that VLX-1005 augmented
321 significantly (P<0.05 by T-test) the magnitude of the gene changes compared to vehicle
322 treatment. Notable genes, whose directional changes are known to counter the interferon

323 response included *Oas1e* (25), *Ttll12* (26), and *Adar* (27) (all upregulated compared to
324 control-treated M1 macrophages), and *Gigyf2* (28) and *Mmp12* (29) (correspondingly
325 downregulated) (**Figure 5G**). These data suggest effects of VLX-1005 that may lead to
326 reduced macrophage interferon signaling.
327
328

329 **DISCUSSION**

330 To date, the adaptive immune system has remained the primary focus for the
331 development of therapeutics aimed at preventing or reversing T1D. Notwithstanding the
332 utility of agents such as anti-CD3 monoclonal antibodies in preserving β cell function (30) or
333 delaying T1D development (7), there has been impetus in the research community to
334 develop therapeutics that target other cell types that contribute to T1D development (31),
335 including innate immune cells and β cells. A multi-targeted approach is expected to aid in
336 better disease modification and result in more durable and broadly applicable therapy (32).
337 In this respect, 12/15-LOX (in mice) is a particularly appealing target since it is active in both
338 macrophages and β cells and contributes to the development of inflammatory disorders,
339 including insulin resistance, atherosclerosis, and T1D (for review, see (9)). The deletion of
340 *Alox15*, specifically in either myeloid cells or islet β cells, proved sufficient to delay/prevent
341 T1D in NOD mice (2, 11). Evidence for 12-LOX contributions to T1D pathogenesis identifies
342 this enzyme as an attractive target in human disease. 12-LOX is elevated in β cells of
343 autoantibody-positive, pre-T1D individuals and in residual β cells of individuals with
344 established T1D (12). A pro-inflammatory product derived from the 12-LOX (and mouse
345 12/15-LOX)-mediated metabolism of arachidonic acid is 12-HETE, an eicosanoid that either
346 directly or indirectly (through G-protein-coupled receptors (33–36)) augments reactive
347 oxygen species generation and endoplasmic reticulum stress in macrophages and islets (37,
348 38). Notably, levels of 12-HETE were shown to be elevated in the circulation of youth and
349 adults with new-onset T1D (compared to healthy controls and those with established T1D)
350 (39).

351 Considering the biological contributions of the 12-LOX enzymes (mouse 12/15-LOX
352 and human 12-LOX) to T1D and other inflammatory disorders, the development of enzyme
353 inhibitors offers an attractive approach to disease modification. Inhibition of 12/15-LOX using
354 ML351 demonstrated promising outcomes in NOD mice, with reductions in insulitis and
355 improvements in glucose homeostasis (13). An inhibitor that showed mouse and human
356 cross-species reactivity, ML127, unfortunately also displayed evidence of off-target

357 cytotoxicity (13). By contrast, VLX-1005 (a.k.a. ML355) is a potent inhibitor (IC_{50} ~300 nM) of
358 human 12-LOX (14) that has shown efficacy in reversing the insulin secretory defects of
359 cytokine-treated human islets in vitro without evidence of cytotoxicity (17); however, the
360 benefit of this inhibitor in disease states in vivo has remained speculative. To address the
361 translational challenge of testing 12-LOX inhibitors in preclinical disease models in vivo, we
362 developed a human gene replacement mouse model on both the C57BL/6J and NOD
363 autoimmune diabetes backgrounds. The utility of this model as a platform for 12-LOX
364 inhibitor testing was confirmed in our multiple low-dose STZ studies, which showed that
365 VLX-1005 administration to *B6.ALOX12* mice precluded hyperglycemia, whereas wild-type
366 controls developed hyperglycemia over time. STZ is a toxin whose full effects involve
367 communication between β cells and macrophages (19), and our findings with systemic
368 administration of VLX-1005 are consistent with similar STZ studies in mice harboring the
369 global deletion of *Alox15* (18)—collectively suggesting that human *ALOX12* gene
370 replacement mice respond appropriately to a 12-LOX inhibitor and that the human *ALOX12*
371 gene can sufficiently replace the functionality of the mouse *Alox15* gene.
372 In recent studies, our group showed that loss of the mouse *Alox15* gene in either
373 myeloid cells or islet β cells could protect animals from the development of autoimmune
374 diabetes on the NOD background (2, 11). The pathological phenotypes of these animals
375 were similar, with reductions in islet invasion by T cells, B cells, and myeloid cells and a
376 characteristic increase in PD-L1 in either macrophages or β cells. PD-L1 is an immune
377 checkpoint protein whose interaction with its receptor PD-1 on adaptive immune cells leads
378 to a more immune-suppressive response (21). In our studies using *NOD.ALOX12* mice, we
379 found similar responses to VLX-1005 treatment, with striking reductions in both innate and
380 adaptive immune cell infiltration into the islets and a notable increase in PD-L1 in the insulitic
381 (immune cell) component. We interpret these latter findings to suggest that the effect of
382 systemically administered VLX-1005 may be greater in macrophages than in β cells. The
383 reductions in markers of β cell proliferation, death, and oxidative stress that we observed
384 with VLX-1005 treatment may also be reflective of this preferential effect on macrophages

385 since these responses are otherwise characteristic of the effects of cytokines on β cells (40).
386 Our RNA-Seq studies of isolated NOD mouse BMDMs polarized to the proinflammatory M1
387 state support this contention, as VLX-1005 treatment resulted in reductions in the interferon
388 response. Our studies open the possibility that VLX-1005 may be useful in autoimmune
389 diabetes resulting from PD-L1 or PD-1 blockade (checkpoint inhibitor therapy) often used to
390 treat cancers (41).

391 Some limitations to our study should be acknowledged. First, because our mouse
392 model replaces the mouse *Alox15* with the human *ALOX12* globally, we cannot be certain
393 that the effects we observed are exclusively related to the inhibition of the human enzyme in
394 only macrophages and β cells; a recent study suggested that mouse *Alox15* may contribute
395 to pro-resolving functions of Tregs (42). It remains unclear, therefore, if the loss of *Alox15*
396 globally in our mouse model might have affected Treg function or the function of other cell
397 types that have low levels of *Alox15* expression. In this respect, our mouse model may have
398 limited utility in other disease states where *ALOX12* might not fully replace the function of
399 *Alox15.* Moreover, we cannot rule out the possibility that *Alox15* and *ALOX12* mediate
400 distinct pathways that nevertheless still allow for shared phenotypes. For example, our RNA
401 sequencing studies of macrophages treated with VLX-1005 reveal distinct reductions in
402 interferon-mediated responses but such effects have not been directly explored as a
403 consequence of *Alox15* in mice. Second, our studies do not fully address the timing and
404 duration of VLX-1005 treatment. We only treated mice for a 4-week period (6-10 weeks of
405 age); it is possible that a longer duration of treatment might have yielded even more robust
406 T1D prevention outcomes. Therefore, the timing and duration of human treatment may
407 require further investigation in our preclinical model. Limitations regarding timing and
408 duration may also apply to diabetes “reversal” studies, in which we observed a reduction in
409 glycemia but no reversal in disease. We cannot rule out the possibility that the effect of VLX-
410 1005 to suppress β cell proliferation may have prevented a more robust outcome in this
411 case. Finally, our study does not assess the potential for 12-LOX inhibition in combination
412 with other immunomodulatory agents. Whereas the relatively modest impact of VLX-1005

treatment in the diabetes reversal studies in *NOD.ALOX12* mice might suggest diminishing returns on the treatment of humans at the time of disease diagnosis, this effect may be amplified in the presence of T or B cell blockade.

Despite these limitations, our studies identify a new platform on which to study a class of LOX inhibitors for their utility in ameliorating human autoimmune diabetes. Our human gene replacement mouse model demonstrates a functional equivalence between mouse *Alox15* and human *ALOX12* in the context of T1D since the whole-body replacement of the mouse gene with the human (under the mouse upstream control elements) preserves islet pathology and the frequency of diabetes incidence in NOD mice. Therefore, beyond its utility to test inhibitors of human 12-LOX, our mouse model also provides a platform to interrogate the cause-effect relationship of human 12-LOX in T1D and possibly other inflammatory diseases in vivo.

426 **MATERIALS and METHODS**

427

428 ***Sex as a biological variable***

429 For *C57BL/6J* mice, our study examined only male mice, because comparative data
430 for these mice in the literature are primarily from males. For *NOD* mice, our study mostly
431 examined females, because type 1 diabetes in the *NOD* strain is more frequently observed
432 in females. However, some data from *NOD* male mice are included that parallel those seen
433 in females, suggesting that the effects observed in females may be relevant to males.

434

435 ***Animals***

436 All experiments involving mice were performed at the University of Chicago and the
437 procedures were conducted according to protocols approved by the University of Chicago
438 Institutional Animal Care and Use Committee. Male and female *C57BL/6J* mice and
439 *NOD/ShiLTJ* mice were procured from the Jackson Laboratory (Bar Harbor, ME). All mice
440 were kept under pathogen free housing conditions with standard light:dark (12:12 h) cycles
441 and fed ad lib normal chow. To generate a humanized *ALOX12* mouse model, the coding
442 region of the mouse *Alox15* gene was replaced with the coding region of the human *ALOX12*
443 gene while retaining all the mouse regulatory elements (**Figure 1A**). Targeted iTL BF1
444 (*C57BL/6* FLP) embryonic stem cells were microinjected into *Balb/c* blastocysts. Chimeras
445 with high percentage of black coat color resulting from this procedure were then mated to
446 *C57BL/6J* wildtype mice to generate germline neo-deleted mice. The following primers were
447 used to genotype the mice: 5'-TCTGATCTGTGTATGCCTGTGTGTGG-3' (forward) and 5'-
448 TTCCAAGGAAAAAGGCATGGTTTCTGAGG-3' (reverse). These primers generate a 478 bp
449 band for wildtype and 581 bp band for knock-in mice (**Supplemental Figure 1A**).

450 Human *ALOX12* alleles were introgressed onto both the *C57BL/6J* and *NOD.ShiLT/J*
451 mouse backgrounds using a speed congenics approach based on microsatellite genotyping
452 at The Jackson Laboratory. Genome scanning was also performed at The Jackson
453 Laboratory to confirm successful backcrossing onto the *C57BL/6J* and *NOD.ShiLT/J* mouse

454 background (*B6.hALOX12* and *NOD.hALOX12*; **Supplemental Table 1** excel file**).** Body
455 mass was measured by EchoMRI.
456 Intraperitoneal glucose tolerance tests (IPGTT) were performed in mice after
457 overnight fasting (16 h). Mice were interperitoneally injected with glucose at a dose of 1 or 2
458 g/kg body weight and blood glucose levels were measured at specific time points: 0, 10, 20,
459 30, 60, 90, and 120 minutes after glucose injection using an AlphaTrak glucometer.
460
461 ***Formulation of VLX-1005***
462 VLX-1005 was obtained from Veralox Therapeutics Inc. A VLX-1005 spray-dried
463 dispersion (for oral administration) was prepared by dissolving VLX-1005 and HPMC-E3 in a
464 90:10 w/w mixture of tetrahydrofuran and water to attain a total solids concentration of 5%
465 w/w. 1575 g of solution was then spray dried using a Buchi B-290 laboratory spray dryer.
466 The yield after spray drying was 67.8 g. The collected material was further dried in an oven
467 at 40 °C under vacuum to remove residual tetrahydrofuran.
468
469 ***Pharmacokinetic Analysis and Lipidomics***
470 Following intraperitoneal injection or oral gavage, VLX-1005 was quantified in plasma
471 using high-performance liquid chromatography-tandem mass spectrometry (Triple Quad
472 6500+; Sciex) after separation by HPLC (Column: Agilient Poroshell 120 EC-C18; HPLC:
473 Shimadzu DGU-405). Pharmacokinetic parameters for VLX-1005 were estimated by non-
474 compartmental model using WinNonlin 8.3. The bioavailability (F%) was calculated as the
475 following: AUC_{last}-PO/AUCINF-PO > 80%: F=(AUCINF-PO*DoseIV)/(mean AUCINF-
476 IV*DosePO). Lipidomics on serum samples was performed by the New York Medical
477 College Lipidomics Core using a Shimadzu LC-MS/MS 8050 system equipped with a
478 UHPLC and auto-sampler.
479
480 ***Streptozotocin (STZ) Induction***

481 Male *C57BL/6J* and *B6.hALOX12* mice (8-10 weeks of age) were injected with either
482 vehicle (0.5% methylcellulose) or 30 mg/kg/day of VLX-1005 by intraperitoneal injection for
483 15 days: 5 days prior to the start of multiple low-dose STZ (55 mg/kg/day; 5 consecutive
484 days), 5 days during STZ treatment, and 5 days post STZ injections. Male *B6.hALOX12*
485 mice (8-10 weeks of age) were injected with either vehicle (0.5% methylcellulose) or 30
486 mg/kg/day of VLX-1005 by oral gavage (PO) for 11 days: 3 days prior to the start of multiple
487 low dose STZ (55 mg/kg/day; 5 consecutive days), 5 days during STZ treatment, and 3 days
488 post STZ injections. Random-fed glucose levels were measured by tail snip using a
489 glucometer (AlphaTrak), and mice were followed for 20 days post-STZ injections. IPGTT
490 was performed on day 4 post-STZ treatments after overnight fasting. At the end of each
491 study, mice were euthanized, and pancreas and blood samples were collected.
492
493 ***Diabetes Incidence and Treatment***
494 Both male and female *NOD.hALOX12* mice were given either vehicle or 30
495 mg/kg/day VLX-1005 (PO) for 4 weeks in the pre-diabetic stage (6-10 weeks of age) and
496 then followed for diabetes incidence until 25 weeks of age or until diabetes diagnosis.
497 Diabetes incidence was determined by observing two consecutive blood glucose values
498 greater than 250 mg/dL. At the end of each study, mice were euthanized, and pancreas and
499 blood samples were collected.
500 For diabetes treatment studies, female *NOD.hALOX12* mice were followed for
501 random-fed blood glucose from 12-20 weeks of age. At diabetes incidence (two consecutive
502 blood glucose values greater than 250 mg/dL), mice were administered 30 mg/kg/day VLX-
503 1005 SDD or vehicle for up to 6 weeks via daily oral gavage or until the mice exhibited signs
504 of physical deterioration from hyperglycemia (loss in body weight, dishevelment). At the end
505 of each study, mice were euthanized, and pancreas and blood samples were collected.
506
507 ***Islet and Macrophage Isolation***

508 Islets were isolated from *NOD.hALOX12* mice with either vehicle or 30 mg/kg/day of
509 VLX-1005treatment using collagenase digestion. Briefly, collagenase was injected into the
510 pancreatic bile duct to digest the connective tissue and release pancreatic cells (43). A
511 Histopaque-HBSS gradient was applied to the dissociated pancreas and centrifuged at 900
512 *xg* for 18 min. The isolated islets were cultured in RPMI medium. The collected islets were
513 handpicked and allowed to recover overnight before processing. RNA was isolated for use in
514 RNA sequencing or quantitative PCR.
515 Bone marrow-derived macrophages (BMDMs) were isolated from 8-week-old
516 *NOD.hALOX12* mice as described previously (2). The isolated BMDMs were cultured for 7
517 days in complete medium (RPMI containing 10% FBS, 10 mM HEPES, and 100 U/ml
518 penicillin/ streptomycin) supplemented with 10 ng/ml M-CSF. On day 7 of culture, the
519 BMDMs were pretreated with either vehicle (0.1% DMSO) or 10 μM VLX-1005. After 1 h
520 pretreatment, the BMDMs were further stimulated with 10 ng/ml LPS and 25 ng/mL IFN-γ for
521 18 h for M1-like polarization. RNA was isolated and used for sequencing.
522
523 ***RNA Isolation and Quantitative PCR***
524 RNA was isolated from mouse tissues and macrophages using an RNeasy Mini® Kit
525 from Qiagen. The isolated RNA was used to synthesize cDNA using a High-Capacity cDNA
526 Reverse Transcription kit (Applied Biosystems) according to manufacturer's instructions.
527 Quantitative PCR was performed using a Bio-Rad CFX Opus with a predesigned Taqman®
528 assay probe for human and mouse genes: human *ALOX12*: Hs00167524_m1; mouse
529 *Alox15*: Mm00507789_m1; mouse *Actb*: Mm01205647_m1 (Invitrogen). The relative gene
530 expression levels were calculated using the comparative threshold cycle value (Ct) and
531 normalized to *Actb*.
532
533 ***Immunostaining, β Cell Mass, and Insulitis Scoring***
534 Pancreatic tissues were fixed using 4% paraformaldehyde. After fixation, the tissues
535 were embedded in paraffin and sectioned with a thickness of 5 μm. Three sections per

536 mouse were used for analysis, with each section being spaced 100 μm apart. Tissue
537 sections were immunostained with anti-insulin (ProteinTech; 15848-1-AP; 1:200), anti-
538 glucagon (Abcam; ab92517; 1:200), anti-12-LOX (Thermo Fisher; PA5-26020; 1:200), anti-
539 12/15-LOX (Abcam; ab80221; 1:200), anti-CD3 (Abcam; ab16669; 1:200), anti-F4/80
540 (Sigma: D2S9R; 1:150), anti-MAC2 (Thermo Fisher; EbioM3/38; 1:200) and anti-H2A.X (Cell
541 Signaling Technology; 9718s; 1:200) primary antibodies followed by conjugated anti-rabbit Ig
542 (Vector Laboratories) secondary antibody. A DAB (3,3'-diaminobenzedine) Peroxidase
543 Substrate Kit from Vector Laboratories was used for detection. After immunostaining, the
544 tissue sections were counterstained with hematoxylin (Sigma). Images were acquired using
545 a BZ-X810 fluorescence microscope (Keyence) and β/α cell mass was quantified by insulin+
546 or glucagon+ area and whole pancreas area. Insulitis score reflects the degree of immune
547 cell infiltration within pancreatic islets. The score system used as follow: 1 = no insulitis, 2 =
548 infiltrate <50% circumference, 3 = infiltrate >50% circumference, 4 = infiltration within islet.
549 Data are shown as the average insulitis score per mouse.
550 For immunofluorescence staining, pancreatic sections were stained with the following
551 antibodies: anti-insulin (Dako IR002; 1:4), anti-glucagon (Santa Cruz; sc514592; 1:50), anti-
552 B220 (Biolegend; 03201; 1:100), anti-CD3 (Abcam; ab16669; 1:200), anti-PCNA (Santa
553 Cruz; sc-7907; 1:100), anti-4HNE (Abcam; ab46545; 1:200), and anti-GPx1(Santa Cruz; sc-
554 22145; 1:100). Highly cross-adsorbed Alexa Fluor secondary antibodies (ThermoFisher)
555 were used at a dilution of 1:500. Tissue sections were stained with DAPI (ThermoFisher) to
556 label cell nuclei. The Nikon A1 confocal microscopy was used to capture images. CellProfiler
557 v4.1 software was used for image analysis.
558
559 ***TUNEL Staining***
560 Terminal deoxynucleotidyl transferase dUTP nick end labelling (TUNEL) assay was
561 used to determine β cell death in pancreatic islets. The assay was performed according to
562 the protocol provided by the manufacturer (Abcam) and HRP-DAB chemistry was used for
563 detection. Two sections, spaced 100 μm apart, were used for each mouse. Images were

564 captured using a BZ-X810 fluorescence microscope system (Keyence). The number of
565 TUNEL+ cells was assessed manually per islet.
566
567 ***NanoString Spatial Proteomics***
568 Paraffin embedded pancreata were used for NanoString spatial proteomics analysis.
569 Tissues were stained with morphology markers: AF-647 conjugated insulin (Cell Signaling;
570 9008s; 1:400) and nuclei marker (SYTO13). Tissues were hybridized using a pre-validated
571 mouse GeoMx Immune cell panel (NanoString; GMX-PROCONCT-MICP) comprising of the
572 following markers: PD-1, CD11c, CD8a, PanCk, MHC II, CD19, CTLA4, SMA, CD11b,
573 CD3e, Fibronectin, Ki-67, CD4, GZMB, F4/80, CD45, PD-L1; housekeeping genes: Histone
574 H3, S6, GAPDH; and IgG antibodies: Rb IgG, Rat IgG2a, and Rat IgG2b for background
575 subtraction. All markers were conjugated to unique UV-photocleavable oligos for indexing. At
576 least 5-6 islets with insulitis were chosen as regions of interest (ROI) per mouse based on
577 the morphology markers (insulin and nuclei). The ROIs were segmented into insulitic region
578 and insulin+ region for each islet. Oligos from the segmented ROIs were photocleaved,
579 collected in a 96-well plate, and reads were counted using nCounter (NanoString). Scaling
580 was performed to normalize for any differences in tissue surface area and depth. After
581 scaling, reads were normalized to housekeeping markers and background was subtracted
582 using IgG markers.
583
584 ***Flow Cytometry***
585 Spleen and pancreatic lymph nodes were harvested, homogenized, and passed
586 through a 70 µm strainer to obtain a single cell suspension. Cell pellets were resuspended in
587 red blood cell (RBC) lysing solution to remove red blood cells. 2.5*10^5- 1*10^6 cells per
588 condition were incubated with blocking solution (eBioscience; 14-0161-86) containing anti-
589 mouse CD16/CD32 to block the Fc receptors for 20 min on ice. The following surface
590 markers were used — CD4- FITC (BioLegend; 100510; 1:100), CD8-PerCP-Cy5.5
591 (Biolegend; 100734; 1:100), CD19-AF700 (Biolegend; 152414; 1:100). Following incubation

592 of surface antibodies, cells were washed with stain buffer and then permeabilized using
593 fix/perm buffer (BD #554722) before intracellular staining. The following intracellular
594 antibodies were used FoxP3-AF647 (BD; 560401; 1:100), IFNγ-PE (BD; 554412; 1:50), and
595 IL17a-APCCY7 (BD; 560821; 1:50). Cells were analyzed on the Attune NxT Flow Cytometer
596 (Thermo Fisher). Data were analyzed by FlowJo software (BD Biosciences).
597
598 ***RNA Sequencing***
599 RNA extraction was performed using RLT Buffer, according to the manufacturer's
600 instructions (Qiagen). Samples were submitted for library generation and sequencing by the
601 University of Chicago sequencing core using a NovaSeq 6000® (Illumina). Data was
602 analyzed using Galaxy (https://usegalaxy.org/). Reads were aligned to the Mus musculus
603 genome build mm10 using HISAT2. Individual sample reads were quantified using HTseq-
604 count and normalized using DESeq2. DEseq2 was also used to calculate fold changes and
605 p-values and perform optional covariate correction. Gene ontology (GO) was used for
606 pathway analysis.
607
608 ***Statistical Methods***
609 All data are represented as mean ± SEM. When comparing more than two
610 conditions, one-way ANOVA was performed. Tukey's post-hoc test or Dunnett's post-hoc
611 test was used to determine specific differences between individual group means. When
612 comparing only two conditions, two-tailed student's t-test was performed. Mantel-Cox log-
613 rank test was specifically used for analyzing the NOD diabetes incidence experiments. Data
614 analyses were performed using the GraphPad Prism 10 software. The differences were
615 considered statistically significant at a p value <0.05.
616
617

618 **ACKNOWLEDGEMENTS**

619 This work was supported in part by National Institutes of Health grants R03
620 TR003381 (to SAT and RGM), R41 DK122917 (to RGM and DJM), R01 DK10558 (to RGM),
621 U01 DK127786 (to RGM), T32 AI153020 (to JRE), an investigator-initiated award from
622 Veralox Therapeutics (to SAT and RGM), a Chicago Biomedical Consortium Director's
623 Award (to RGM), and Breakthrough T1D postdoctoral fellowship (3-PDF-2023-1326-A-N)
624 and Diabetes Research Connection awards (both to CM). This study utilized Diabetes
625 Center core resources supported by National Institutes of Health grant P30 DK020595 (to
626 the University of Chicago) and utilized services of the University of Chicago Histology and
627 Genomics Cores.

628

629 **AUTHOR CONTRIBUTIONS**

630 JLN, DJM, MBB, SAT, and RGM conceptualized the research; TN, CM, JRE, JEW,
631 AC, KF, SP, JBN, and SAT performed investigation; SAT and RGM provided project
632 supervision; TN, SCM, SAT, and RGM wrote the original draft; all authors contributed to
633 discussion, edited the manuscript, and approved the final version of the manuscript.

634

635 **DATA AVAILABILITY**

636 The islet RNA sequencing data have been uploaded to the Gene Expression
637 Omnibus (https://www.ncbi.nlm.nih.gov/geo/) with accession number GSE272668. The
638 BMDM sequencing data have been uploaded to the Gene Expression Omnibus with
639 accession number GSE272687. Any additional information required to reanalyze the data
640 reported in this paper is available from the corresponding author upon request.

641

642 **DECLARATION OF INTERESTS**

643 RGM and SAT received an investigator-initiated award from Veralox Therapeutics.
644 RGM serves on the Scientific Advisory Board for Veralox Therapeutics. DJM and MBB are
645 Veralox Therapeutics employees.

647 **REFERENCES**

648

649 1. Atkinson MA, Mirmira RG. The pathogenic “symphony” in type 1 diabetes: A disorder of
650 the immune system, β cells, and exocrine pancreas. *Cell Metab*. 2023;S1550-
651 4131(23)00228–0.

652 2. Kulkarni A, et al. 12-Lipoxygenase governs the innate immune pathogenesis of islet
653 inflammation and autoimmune diabetes. *JCI Insight*. 2021;6(14):147812.

654 3. Lee H, et al. Beta Cell Dedifferentiation Induced by IRE1α Deletion Prevents Type 1
655 Diabetes. *Cell Metab*. 2020;31(4):822-836.e5.

656 4. Tersey SA, et al. Islet β-cell endoplasmic reticulum stress precedes the onset of type 1
657 diabetes in the nonobese diabetic mouse model. *Diabetes*. 2012;61(4):818–827.

658 5. Gonzalez-Duque S, et al. Conventional and Neo-antigenic Peptides Presented by β Cells
659 Are Targeted by Circulating Naïve CD8+ T Cells in Type 1 Diabetic and Healthy Donors. *Cell*
660 *Metab*. 2018;28(6):946-960.e6.

661 6. Roep BO, et al. Type 1 diabetes mellitus as a disease of the β-cell (do not blame the
662 immune system?). *Nat Rev Endocrinol*. 2021;17(3):150–161.

663 7. Herold KC, et al. An Anti-CD3 Antibody, Teplizumab, in Relatives at Risk for Type 1
664 Diabetes. *N Engl J Med*. 2019;381(7):603–613.

665 8. Dobrian AD, et al. Functional and pathological roles of the 12- and 15-lipoxygenases.
666 *Prog Lipid Res*. 2011;50:115–131.

667 9. Kulkarni A, et al. Regulation of Tissue Inflammation by 12-Lipoxygenases. *Biomolecules*.
668 2021;11(5):717.

669 10. McDuffie M, et al. Nonobese diabetic (NOD) mice congenic for a targeted deletion of
670 12/15-lipoxygenase are protected from autoimmune diabetes. *Diabetes*. 2008;57(1):199–
671 208.

672 11. Piñeros AR, et al. Proinflammatory signaling in islet β cells propagates invasion of
673 pathogenic immune cells in autoimmune diabetes. *Cell Rep*. 2022;39(13):111011.

674 12. Grzesik WJ, et al. Expression pattern of 12-lipoxygenase in human islets with type 1
675 diabetes and type 2 diabetes. *J Clin Endocrinol Metab*. 2015;100(3):E387-395.

676 13. Hernandez-Perez M, et al. Inhibition of 12/15-Lipoxygenase Protects Against β-Cell
677 Oxidative Stress and Glycemic Deterioration in Mouse Models of Type 1 Diabetes. *Diabetes*.
678 2017;66(11):2875–2887.

679 14. Luci D, et al. Discovery of ML355, a Potent and Selective Inhibitor of Human 12-
680 Lipoxygenase. *Probe Reports from the NIH Molecular Libraries Program*. Bethesda (MD):
681 National Center for Biotechnology Information (US); 2010.

682 15. Rai G, et al. Discovery of ML351, a Potent and Selective Inhibitor of Human 15-
683 Lipoxygenase-1. *Probe Reports from the NIH Molecular Libraries Program*. Bethesda (MD):
684 National Center for Biotechnology Information (US); 2010.

685 16. Luci DK, et al. Synthesis and structure-activity relationship studies of 4-((2-hydroxy-3-
686 methoxybenzyl)amino)benzenesulfonamide derivatives as potent and selective inhibitors of
687 12-lipoxygenase. *J Med Chem*. 2014;57(2):495–506.

688 17. Ma K, et al. 12-Lipoxygenase Inhibitor Improves Functions of Cytokine-Treated Human
689 Islets and Type 2 Diabetic Islets. *J Clin Endocrinol Metab*. 2017;102(8):2789–2797.

690 18. Bleich D, et al. Resistance to type 1 diabetes induction in 12-lipoxygenase knockout
691 mice. *J Clin Invest*. 1999;103:1431–1436.

692 19. Calderon B, et al. Dendritic cells in islets of Langerhans constitutively present beta cell-
693 derived peptides bound to their class II MHC molecules. *Proc Natl Acad Sci U S A*.
694 2008;105(16):6121–6126.

695 20. Anderson MS, Bluestone JA. The NOD mouse: a model of immune dysregulation. *Annu*
696 *Rev Immunol*. 2005;23:447–485.

697 21. Falcone M, Fousteri G. Role of the PD-1/PD-L1 Dyad in the Maintenance of Pancreatic
698 Immune Tolerance for Prevention of Type 1 Diabetes. *Front Endocrinol (Lausanne)*.
699 2020;11:569.

700 22. Gagnerault M-C, et al. Pancreatic Lymph Nodes Are Required for Priming of β Cell
701 Reactive T Cells in NOD Mice. *Journal of Experimental Medicine*. 2002;196(3):369–377.

702 23. Evans-Molina C, et al. PPAR-{gamma} Activation Restores Islet Function in Diabetic
703 Mice Through Reduction of ER Stress and Maintenance of Euchromatin Structure. *Mol Cell*
704 *Biol*. 2009;29:2053–2067.

705 24. Tersey SA, et al. 12-Lipoxygenase Promotes Obesity-Induced Oxidative Stress in
706 Pancreatic Islets. *Mol Cell Biol*. 2014;34(19):3735–3745.

707 25. Harioudh MK, et al. The canonical antiviral protein oligoadenylate synthetase 1 elicits
708 antibacterial functions by enhancing IRF1 translation. *Immunity*. 2024;57(8):1812-1827.e7.

709 26. Ju L-G, et al. TTLL12 Inhibits the Activation of Cellular Antiviral Signaling through
710 Interaction with VISA/MAVS. *J Immunol*. 2017;198(3):1274–1284.

711 27. Knebel UE, et al. Disrupted RNA editing in beta cells mimics early-stage type 1 diabetes.
712 *Cell Metab*. 2024;36(1):48-61.e6.

713 28. Xu Z, et al. SARS-CoV-2 impairs interferon production via NSP2-induced repression of
714 mRNA translation. *Proc Natl Acad Sci U S A*. 2022;119(32):e2204539119.

715 29. Dufour A, et al. C-terminal truncation of IFN-γ inhibits proinflammatory macrophage
716 responses and is deficient in autoimmune disease. *Nat Commun*. 2018;9(1):2416.

717 30. Herold KC, et al. Anti-CD3 monoclonal antibody in new-onset type 1 diabetes mellitus. *N*
718 *Engl J Med*. 2002;346:1692–1698.

719 31. von Herrath M, et al. Anti-interleukin-21 antibody and liraglutide for the preservation of β-
720 cell function in adults with recent-onset type 1 diabetes: a randomised, double-blind,
721 placebo-controlled, phase 2 trial. *Lancet Diabetes Endocrinol*. 2021;9(4):212–224.

722 32. Long SA, Speake C. Combination therapy in recent-onset type 1 diabetes. *Lancet*
723 *Diabetes Endocrinol*. 2021;9(4):191–193.

724 33. Ermis E, et al. Leukotriene B4 receptor 2 governs macrophage migration during tissue
725 inflammation. *J Biol Chem*. 2024;300(1):105561.

726 34. Guo Y, et al. Identification of the orphan G protein-coupled receptor GPR31 as a
727 receptor for 12-(S)-hydroxyeicosatetraenoic acid. *J Biol Chem*. 2011;286:33832–33840.

728 35. Hernandez-Perez M, et al. A 12-lipoxygenase-Gpr31 signaling axis is required for
729 pancreatic organogenesis in the zebrafish. *FASEB J*. 2020;34(11):14850–14862.

730 36. Yokomizo T, et al. Hydroxyeicosanoids bind to and activate the low affinity leukotriene
731 B4 receptor, BLT2. *J Biol Chem*. 2001;276(15):12454–12459.

732 37. Chen M, et al. Activation of 12-lipoxygenase in proinflammatory cytokine-mediated beta
733 cell toxicity. *Diabetologia*. 2005;48:486–495.

734 38. Weaver JR, et al. Integration of pro-inflammatory cytokines, 12-lipoxygenase and NOX-1
735 in pancreatic islet beta cell dysfunction. *Mol Cell Endocrinol*. 2012;358(1):88–95.

736 39. Hennessy E, et al. Elevated 12-hydroxyeicosatetraenoic acid (12-HETE) levels in serum
737 of individuals with newly diagnosed Type 1 diabetes. *Diabet Med*. 2017;34(2):292–294.

738 40. Eizirik DL, Colli ML, Ortis F. The role of inflammation in insulitis and beta-cell loss in type
739 1 diabetes. *Nat Rev Endocrinol*. 2009;5(4):219–226.

740 41. Chen X, et al. Immune Checkpoint Inhibitors and Risk of Type 1 Diabetes. *Diabetes*
741 *Care*. 2022;45(5):1170–1176.

742 42. Marques RM, et al. Loss of 15-lipoxygenase disrupts Treg differentiation altering their
743 pro-resolving functions. *Cell Death Differ*. 2021;28(11):3140–3160.

744 43. Stull ND, et al. Mouse islet of Langerhans isolation using a combination of purified
745 collagenase and neutral protease. *J Vis Exp*. 2012;(67):4137.

746

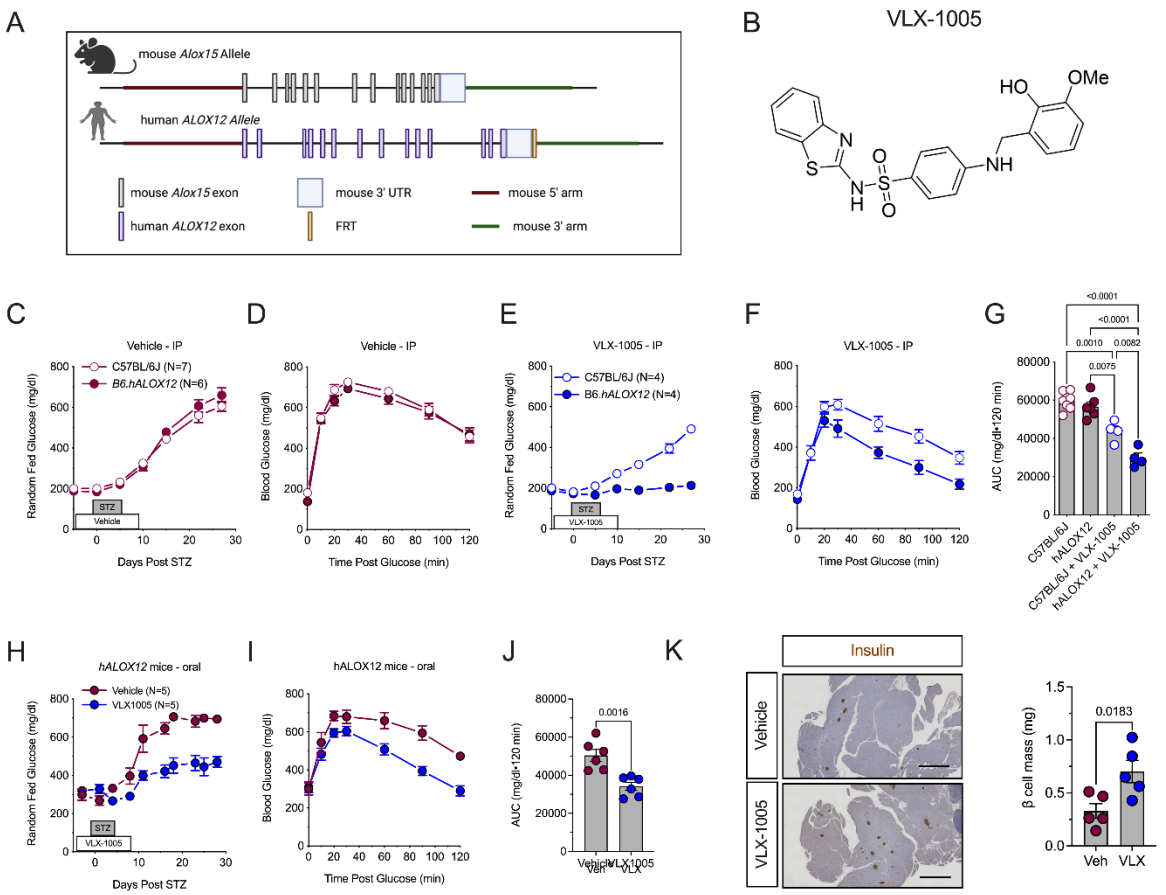

Figure 1: 12-LOX inhibition protects against streptozotocin-induced diabetes. *C57BL/6J* and *B6.hALOX12* male mice (N=4-7 per group as indicated) were treated with 30 mg/kg intraperitoneal or PO VLX-1005 and multiple low-dose streptozotocin (STZ). (**A**) Schematic of the generation of *hALOX12* mice by replacing mouse *Alox15* with human *ALOX12*. (**B**) Chemical structure of VLX-1005. (**C**) Random-fed blood glucose values in vehicle-treated male *C57BL/6J* and *B6.hALOX12* mice after STZ. (**D**) GTT of vehicle-treated male *C57BL/6J* and *B6.hALOX12* mice after STZ at day 4 post-STZ-treatment. (**E**) Random-fed blood glucose values in VLX-1005-treated male *C57BL/6J* and *B6.hALOX12* mice after STZ. (**F**) GTT of VLX-1005-treated male *C57BL/6J* and *B6.hALOX12* mice after STZ at day 4 post-STZ-treatment. (**G**) AUC of *C57BL/6J* and *B6.hALOX12* after STZ at day 4 post-STZ-treatment (one-way ANOVA). (**H**) Random-fed blood glucose values in male vehicle- or VLX-1005-treated (PO) *B6.hALOX12* mice after STZ. (**I**) GTT of male vehicle- or VLX-1005-treated (PO) *B6.hALOX12* mice after STZ at day 4 post-STZ-treatment. (**J**) AUC of *B6.hALOX12* after STZ at day 4 post-STZ-treatment. (**K**) Pancreata stained for insulin (left panel) and β cell mass measurement (right panel) from male *B6.hALOX12* mice at day 26 post-STZ-treatment. Scale bars = 500 μm. Data are presented as mean ±SEM and statistical significance was determined by a two-tailed T-test or one-way ANOVA.

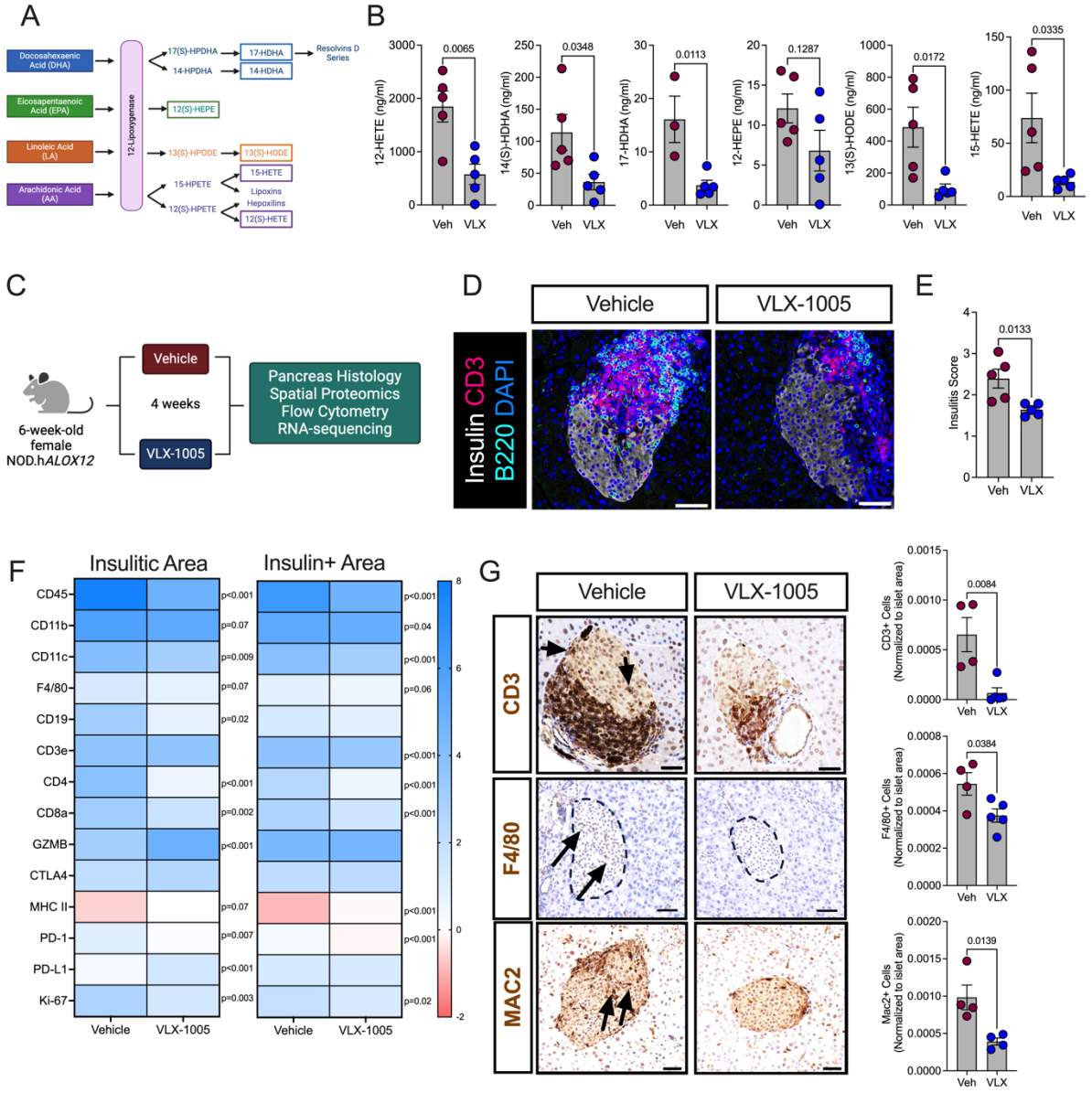

Figure 2: VLX-1005 decreased islet inflammation in *NOD.hALOX12* female mice. 6-week-old female pre-diabetic *NOD.ALOX12* mice were treated orally with 30 mg/kg VLX-1005 for 4 weeks prior to tissue analysis. (**A**) Schematic representation of 12-lipoxygenase products. (**B**) Serum lipidomics results of 12-lipoxygnease products as indicated. (**C**) Schematic representation of mouse treatment paradigm. (**D**) Pancreata from mice stained for CD3 (magenta), B220 (teal), insulin (white), and nuclei (blue). Scale bars = 50 µm. (**E**) Average insulitis score, each dot represents an individual mouse. (**F**) Heatmap of identified proteins in the insulitic area (*left panel*) and insulin-positive area (*right panel*). (**G**) Pancreata of mice stained and quantified for CD3 (brown, *top panels*; *arrows* indicate positive CD3 staining within the islet), F4/80 (brown, *middle panels*; *arrows* indicate positive F4/80 staining within the islet), or MAC2 (brown, *bottom panels*; *arrows* indicate positive MAC2 staining within the islet) and nuclei (blue). Scale bars = 50 µm. Data are presented as mean ±SEM and statistical significance was determined by a two-tailed T-test in all cases.

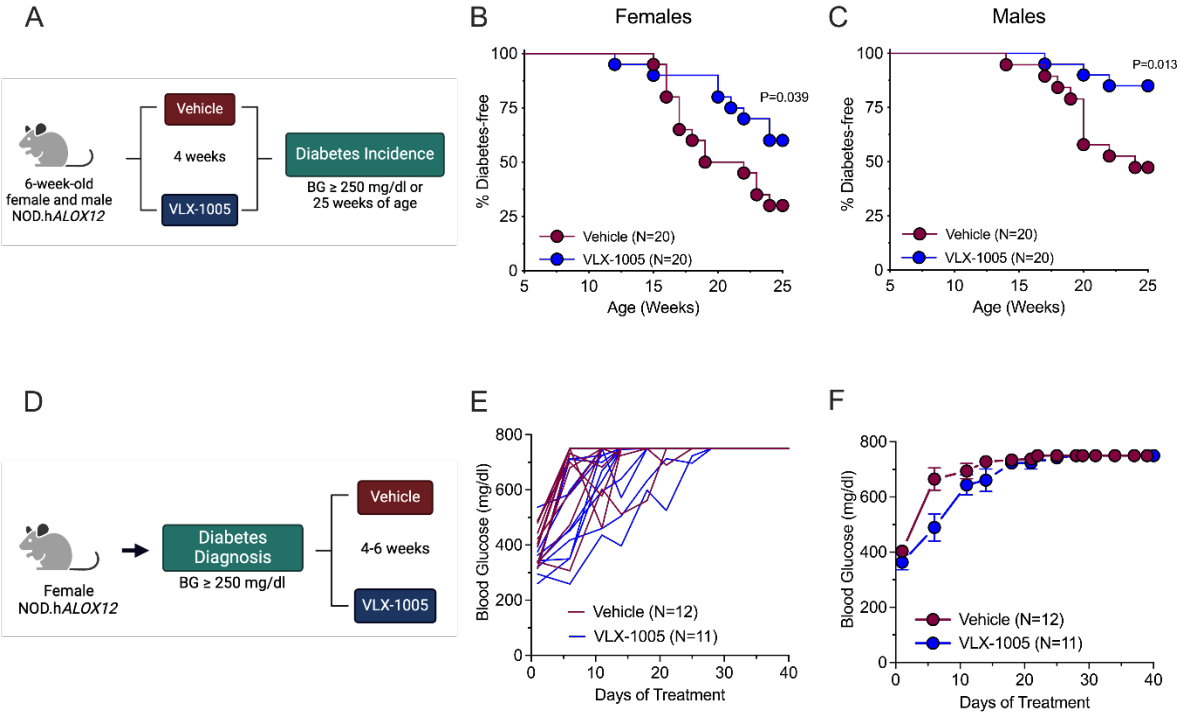

Figure 3: VLX-1005 treatment delays autoimmune diabetes onset in female and male *NOD.hALOX12* mice. *NOD.hALOX12* mice (N=20 per group) were treated during the pre-diabetic stage from 6-10 weeks of age or at the time of diabetes development (N=11-12 per group). (**A**) Schematic representation of diabetes prevention experimental design. (**B**) Diabetes incidence in female *NOD.hALOX12* mice. (**C**) Diabetes incidence in male *NOD.hALOX12* mice. (**D**) Schematic representation of diabetes reversal experimental design. (**E**) Random-fed blood glucose levels in each female mouse. (**F**) Average random-fed blood glucose levels of female mice. Data are presented as mean ±SEM and statistical significance was determined by a Mantel-Cox Log Rank test.

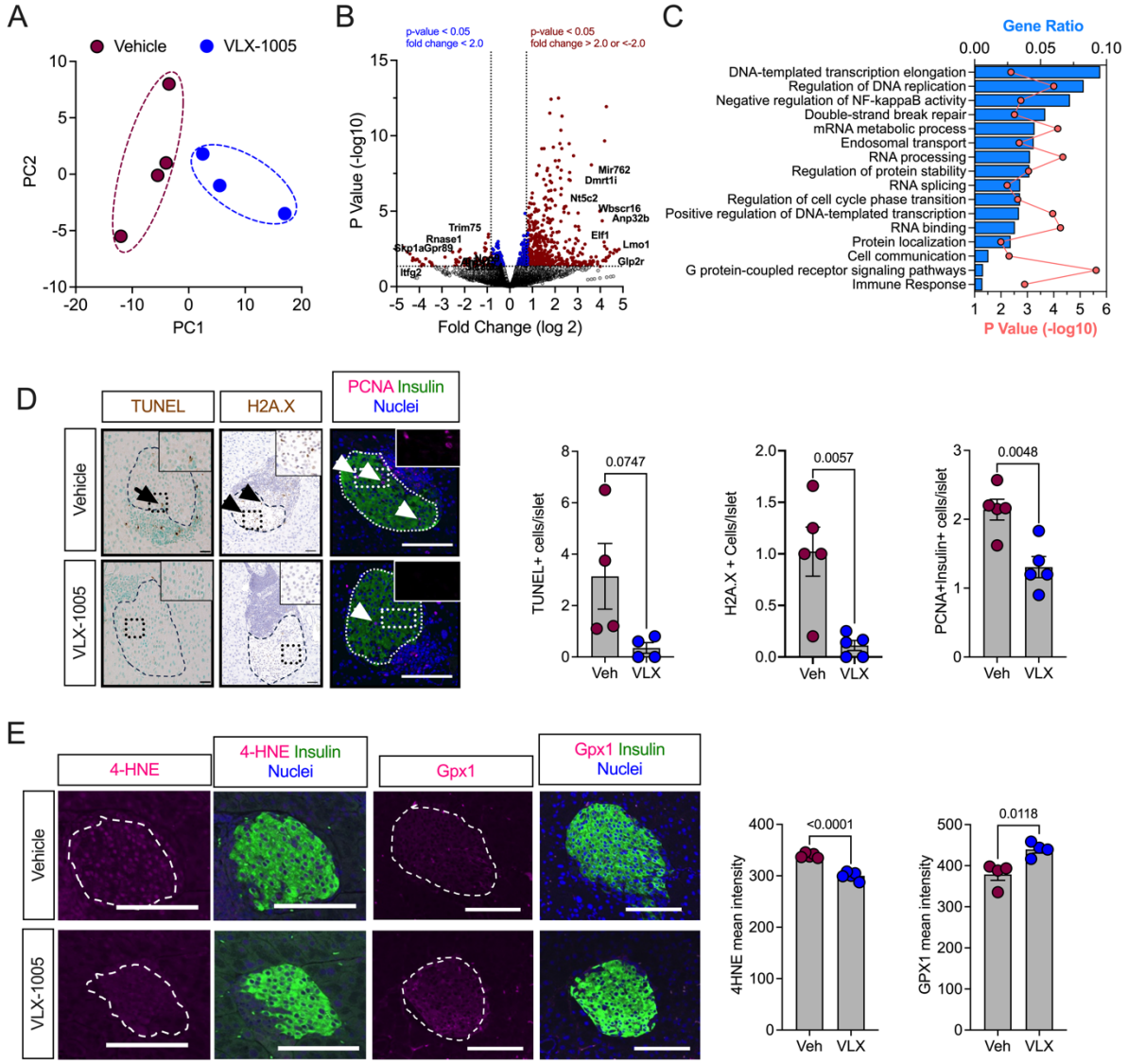

Figure 4: VLX-1005 decreased β cell death, proliferation, and oxidative stress in female *NOD.hALOX12* mice. Pancreata or islets were harvested from 10-week-old prediabetic female *NOD.hALOX12* mice after 4 weeks of treatment with vehicle or VLX-1005 (N=4 per group). (**A**) Principal component analysis plot of RNA-sequencing results from isolated islets of vehicle- or VLX-1005-treated mice. (**B**) Volcano plot of differentially expressed genes. (**C**) Gene ontology pathway analysis of differentially expressed genes. (**D**) Pancreata from mice stained and quantified for TUNEL (brown, *left panels*; black *arrow* indicates positive TUNEL staining within the islet), H2A.X (brown, *middle panels*; black *arrowheads* indicate positive H2A.X staining within the islet), or PCNA (magenta, *right panels*; white *arrowheads* indicate positive PCNA staining within the islet), insulin (green) and nuclei (blue). Scale bars = 50 µm. (**E**) Pancreata from mice stained and quantified for 4-HNE (magenta, *left panels*), or GPx1 (magenta, *right panels*), and insulin (green) and nuclei (blue). Scale bars = 50 µm. Data are presented as mean ±SEM and statistical significance was determined by a two-tailed T-test.

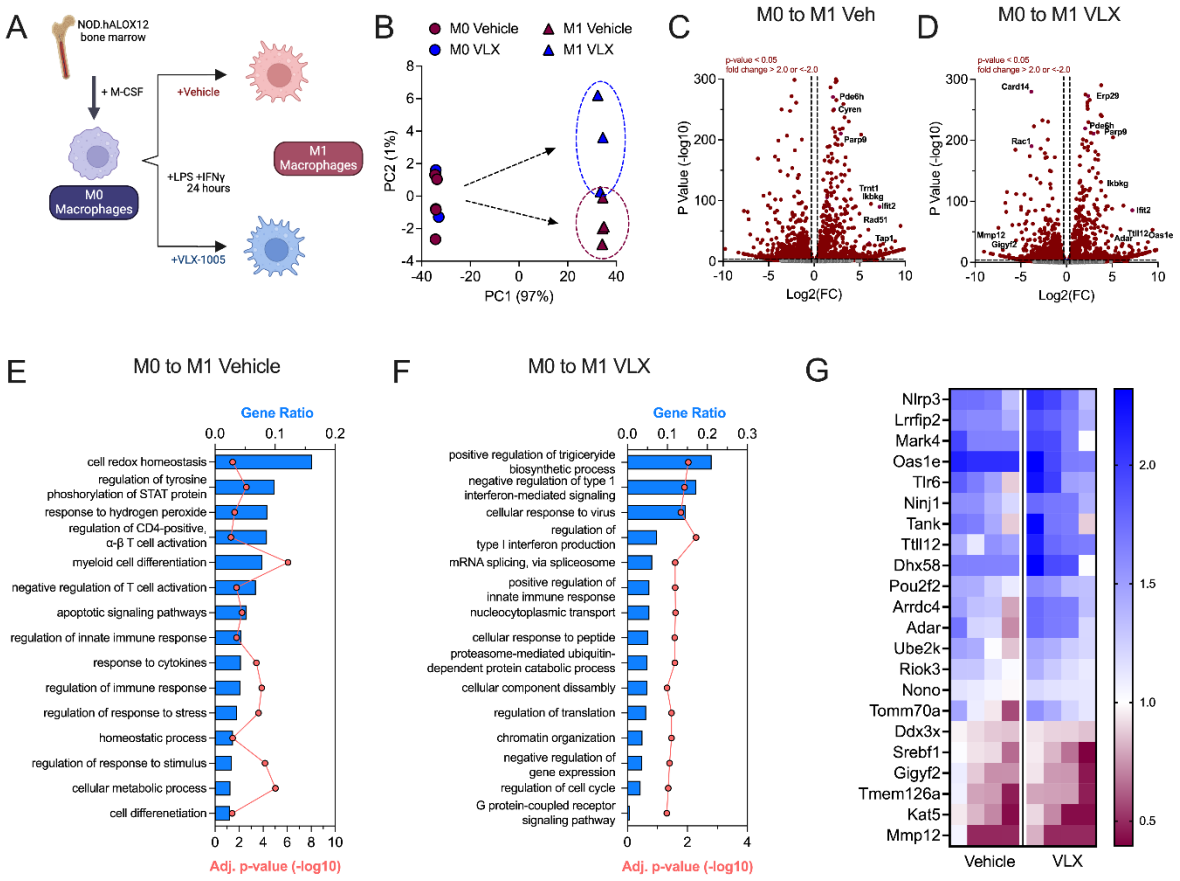

Figure 5: RNA-sequencing analysis of M1-like bone marrow derived macrophages reveals a reduction in the inflammatory response upon VLX-1005 treatment. Bone marrow-derived macrophages (BMDMs) were isolated and polarized to the M1-like state and treated with vehicle or VLX-1005 (10 μM) during polarization. RNA was isolated and sequenced. (**A**) Schematic of experimental design. (**B**) Principal component analysis plot. (**C**) Volcano plot of differentially expressed genes in M0 and M1-like vehicle-treated macrophages. (**D**) Volcano plot of differentially expressed genes in M0 and M1-like VLX-1005-treated macrophages. (**E**) Gene ontology pathway analysis of differentially expressed genes in M0 vs M1-like vehicle-treated macrophages. (**F**) Gene ontology pathway analysis of differentially expressed genes in M0 vs M1-like VLX-1005-treated macrophages. (**G**) Heatmap of significantly altered interferon-related genes. Columns represent sequencing results from each sample (N=4 per group). Numbers on the heatmap scale indicate fold change compared to M0 macrophages.

828 **Table 1: RNA expression levels of human *ALOX12* and mouse *Alox15* normalized to**

829 **mouse *Actb* from various isolated tissues of *C57BL/6J* and *B6.hALOX12* mice.**

830

Mouse Strain	Tissues	*ALOX12* (ΔCT)	*Alox15* (ΔCT)
C57BL/6J	Islets	ND	7.66 ± 0.32
	Spleen	ND	18.41 ± 1.31
	BMDM	ND	17.47 ± 0.03
	Peritoneal Macrophages	ND	3.62 ± 0.26
	Liver	ND	12.2 ± 1.77
	Kidney	ND	15.02 ± 0.09
	Lung	ND	9.65 ± .063
	Fat	ND	10.84 ± 0.55
B6.hALOX12	Islets	7.91 ± 0.18	ND
	Spleen	14.11 ± 0.26	ND
	BMDM	14.48 ± 0.47	ND
	Peritoneal Macrophages	6.06 ± 0.16	ND
	Liver	13.88 ± 0.32	ND
	Kidney	10.12 ± 0.10	ND
	Lung	13.68 ± 0.32	ND
	Fat	8.05 ± 0.42	ND

831 ND = not detected.

832

833 **Table 2: Plasma concentration vs time profile for VLX-1005 after 30 mg/kg PO in**
834 ***C57BL/6J* mice and *NOD.ShiLt/J* mice.**
835

	C57BL/6J		NOD.ShiLt/J	
Pharmacokinetic Parameter	Mean ± SD	CV (%)	Mean ± SD	CV (%)
*$T_{1/2}$ (h)	3.24 ± 0.07	2.17	2.53 ± 0.41	16.1
T_{max} (h)	0.250 ± 0.00	0.00	0.250 ± 0.00	0.000
C_{max} (ng/ml)	13300 ± 624	4.70	14253 ± 5474	38.4
AUC_{last} (h*ng/ml)	15029 ± 3177	21.1	13211 ± 1631	12.3
AUC_{Inf} (h*ng/ml)	15083 ± 3206	21.3	13225 ± 1625	12.3
$AUC_{_\%Extrap_obs}$ (%)	0.342 ± 0.133	38.9	0.115 ± 0.099	85.6
MRT_{Inf_obs} (h)	2.57 ± 0.38	14.8	3.81 ± 0.71	18.7
AUC_{last}/D (h*ng/ml)	501 ± 106	21.1	440 ± 54	12.3

848
849 *$T_{1/2}$, half life; T_{max}, time to maximium drug concentration; C_{max}, maximum drug concentration; AUC_{last}, area under
850 the curve from the time of dosing to the last measurable concentration; AUC_{inf}, area under the curve from the
851 time of dosing extrapolated to infinity; $AUC_{\%extrapobs}$, area under the curve from the time of dosing extrapolated to
852 last observed concentration; MRT_{inf_obs}, mean residence time from the time of dosing extrapolated to infinity;
853 $AUC_{last/D}$, dose normalized area under the curve to time of last measurable concentration.